Investigation of White Matter Networks in Resting State BOLD fMRI

By

Alexa L. Eby

Thesis

Submitted to the Faculty of the

Graduate School of Vanderbilt University

In partial fulfillment of the requirements

For the degree of

MASTER OF SCIENCE

in

Electrical and Computer Engineering

May 10, 2024

Nashville, Tennessee

Approved:

Bennett A. Landman, PhD

Mitchell D. Wilkes, PhD

ACKNOWLEDGEMENTS

This work is supported by National Institutes of Health (1RF1MH123201, R01NS113832, R01EB017230, 1K01EB032898), Vanderbilt Discovery Grant (FF600670), grant of Vanderbilt Institute for Clinical and Translational Research (UL1TR0002243). This work was conducted in part using the resources of the Advanced Computing Center for Research and Education at Vanderbilt University, Nashville, TN. The Vanderbilt Institute for Clinical and Translational Research (VICTR) is funded by the National Center for Advancing Translational Sciences (NCATS) Clinical Translational Science Award (CTSA) Program, Award Number 5UL1TR002243-03. The content is solely the responsibility of the authors and does not necessarily represent the official views of the NIH.Data collection and sharing for ADNI were supported by National Institutes of Health Grant U01-AG024904 and Department of Defense (award number W81XWH-12-2-0012). ADNI is also funded by the National Institute on Aging, the National Institute of Biomedical Imaging and Bioengineering, and through generous contributions from the following: AbbVie, Alzheimer's Association; Alzheimer's Drug Discovery Foundation; Araclon Biotech; BioClinica, Inc.; Biogen; Bristol-Myers Squibb Company; CereSpir, Inc.; Cogstate; Eisai Inc.; Elan Pharmaceuticals, Inc.; Eli Lilly and Company; EuroImmun; F. Hoffmann-La Roche Ltd and its affiliated company Genentech, Inc.; Fujirebio; GE Healthcare; IXICO Ltd.; Janssen Alzheimer Immunotherapy Research & Development, LLC.; Johnson & Johnson Pharmaceutical Research & Development LLC.; Lumosity; Lundbeck; Merck & Co., Inc.; Meso Scale Diagnostics, LLC.; NeuroRx Research; Neurotrack Technologies; Novartis Pharmaceuticals Corporation; Pfizer Inc.; Piramal Imaging; Servier; Takeda Pharmaceutical Company; and Transition Therapeutics. The Canadian Institutes of Health Research is providing funds to support ADNI clinical sites in Canada. Private sector contributions are facilitated by the Foundation for the National Institutes of Health (www.fnih.org). The grantee organization is the Northern California Institute for Research and Education, and the study is coordinated by the Alzheimer's Therapeutic Research Institute at the University of Southern California. ADNI data are disseminated by the Laboratory for Neuro Imaging at the University of Southern California. The ADNI cohort (https://adni.loni.usc.edu) began in 2003 as a public-private partnership, led by Principal Investigator, Michael W. Weiner, MD, Jack Jr CR, Bernstein MA, Fox NC, et al. The Alzheimer's disease neuroimaging initiative (ADNI): MRI methods. Journal of Magnetic Resonance Imaging: An Official Journal of the International Society for Magnetic Resonance in Medicine. 2008;27(4):685-691. The BLSA is supported by the Intramural Research Program, National Institute on Aging, NIH.Data were provided in part by OASIS for the OASIS-3 cohort: Longitudinal Multimodal Neuroimaging: Principal Investigators: T. Benzinger, D. Marcus, J. Morris; NIH P30 AG066444, P50 AG00561, P30 NS09857781, P01 AG026276, P01 AG003991, R01 AG043434, UL1 TR000448, R01 EB009352. AV-45 doses were provided by Avid Radiopharmaceuticals, a wholly owned subsidiary of Eli Lilly. HCP: Data were provided [in part] by the Human Connectome Project, WU- Minn Consortium (Principal Investigators: David Van Essen and Kamil Ugurbil; 1U54MH091657) funded by the 16 NIH Institutes and Centers that support the NIH Blueprint for Neuroscience Research; and by the McDonnell Center for Systems Neuroscience at Washington University. The content is solely the responsibility of the authors and does not necessarily represent the official views of the NIH.

TABLE OF CONTENTS

LIST OF FIGURES

Figure **Page**

INTRODUCTION

A common noninvasive technique used to measure neuronal activity is blood oxygen level dependent functional magnetic resonance imaging (BOLD-fMRI) [1]. It measures the spontaneous hemodynamic responses in blood, where an increase in blood to a neuron in a brain region, indicates an increase in neuronal activity [1][2]. Resting state BOLD-fMRI is used to investigate default functional signals while the brain is not subjected to any external stimuli [3]. Commonly, in resting state scans only grey matter is investigated and used to create functional mappings of the brain [3]. This functional mapping is important for understanding aging effects and diseases, such as Alzheimer's Disease [4][5].

Commonly, grey matter is much more voluminous and has a larger BOLD signal at resting state compared to white matter BOLD signals. As a result of these large differences in signal, the white matter BOLD signals are discounted or considered noise and regressed out with the global signal in preprocessing [6][7]. However, there is growing evidence these white matter signals can provide insight into functional brain regions [7]. Recent literature has begun investigating the significance of resting state white matter signals and found that the hemodynamic responses of white matter and grey matter are similar in shape, and only the magnitude of the hemodynamic response in white matter differ [7][8].

To quantify the correlations in white matter, recent studies have begun clustering the signals to identify similar correlations, or networks, within the brain. To cluster, previous work has used k-means clustering techniques only and has revealed clusters that have relative stability within a small subject population [9][10]. When performing clustering with more subjects, there are also clear spatial patterns that are revealed for each dataset. As a result, it is hypothesized that white matter signals are reproducible across different subject populations at different acquisition sites or datasets (Figure 1). This work leverages hierarchical clustering to investigate clustering on BOLD-fMRI white matter correlations using three different large subject population datasets.

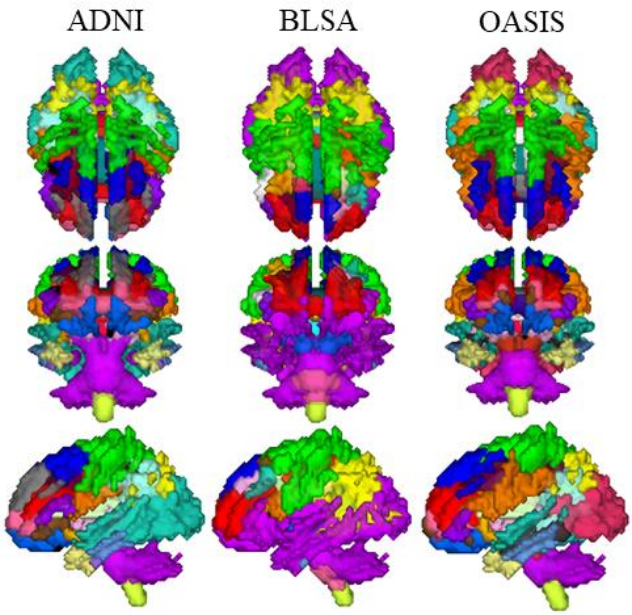

Figure 1 White Matter Clusters Across Datasets. Spatially organized white matter networks in resting state BOLD-fMRI are identified through hierarchical clustering of the average voxel wise correlations within a dataset. These white matter networks exhibit spatial patterns within a dataset that are not generated by chance ($P<0.001$). In this study, it is hypothesized that the white matter networks are reproducible across subject populations that are acquired at different acquisition sites.

METHODS

Datasets

Three different databases, Open Access Series of Imaging Studies-3 (OASIS) database [11], Alzheimer's Disease Neuroimaging Initiative (ADNI) database [12], and Baltimore Longitudinal Study of Aging (BLSA) database [13], with different subject populations in each site are used. All subjects are cognitively normal (clinical dementia rating = 0), scanned in a single session, and there are approximately an equal number of males and females. Also, all data were deidentified. From the OASIS database 734 subjects and 734 resting state fMRI scans (acquired at 4mm x 4mm x 4mm resolution with a time to echo=0.027 S and repetition time=2.2 S) with ages between 47.5 and 95.3 years old were used. Many individuals provide longitudinal data and most subjects were scanned twice in a given session, but only the first scan from the first session was used for this analysis. Images were acquired every second over a 164 second interval [11].

From the ADNI database*, 333 subjects and 485 resting state fMRI scans (acquired at 3mm x 3mm x 3.973mm resolution with a time to echo=0.03 S and repetition time=2 S) with ages between 65.3 and 91.5 years old were used. Like in the OASIS dataset, subjects provide longitudinal data and within the first session multiple scans were acquired. Here the first two scans from the first session were used because there were fewer subjects in ADNI compared to the other two datasets. The subject does not leave the scanner between the first and second scan, and it is assumed that both scans are providing resting state data reflecting the subjects brain activity at the given point in longitudinal time and should not be changing between the two scans. Images were acquired every second, and the length of each image acquisition varied for each scan ranging being 140 to 976 seconds [12].

From the BLSA database, 876 subjects and 876 resting state fMRI scans (acquired at 3.4375mm x 3.4375mm x 3.4mm resolution with a time to echo=0.0320 S and repetition time=3 S) with ages between 22.4 and 103 years old were used. Only the first scan from the first session for each subject was used. The length of image acquisition was 187 seconds, with images being acquired in one second intervals [13].

Image Processing

Scans from all three databases were processed using a customized white matter pipeline, specifically made to capture the small quantitative white matter BOLD signal changes [14]. Briefly, slice timing and head motion were removed from the volumes. Then, the mean cerebrospinal fluid signal and 24 motion-related parameters were modeled as covariates and regressed out from the BOLD signals. The data were detrended and passed through a temporal filter with a passband frequency between 0.01 and 0.1 Hz. These procedures were completed in the white matter pipeline using a customized version of the DPABI toolbox [14] [15]. All subject scans were spatially normalized into MNI space (voxel size equal to $3x3x3mm^3$) using SPM12 [16]. Lastly, grey matter, white matter, and cerebrospinal fluid tissues were segmented using the Computational Anatomy Toolbox [17]. The segmentation was completed based on the tissue probability maps derived from each subject's T1-weighted image. Lastly, all images were subjected to quality assurance. The criteria included (1) all preprocessed results are successfully generated; (2) the maximum head motion translation is 2 mm and maximum head motion rotation is 2 deg; (3) the mean frame-wise displacement is less than 0.5 mm; (4) the spatial normalization was acceptable by visual inspection [14][18].

For analysis, a dataset level average subject white matter mask and a total across dataset average subject white matter mask was created. For each subject, a white matter mask is derived from the subject specific white matter tissue probability map.

*Data used in preparation of this article were derived from BIOCARD study data, supported by grant U19 – AG033655 from the National Institute on Aging. The BIOCARD study team did not participate in the analysis or writing of this report, however, they contributed to the design and implementation of the study. A listing of BIOCARD investigators may be accessed at: https://www.biocard-se.org/public/Core%20Groups.html

All subject white matter masks are overlaid, and a threshold is applied to create an average white matter mask. A threshold of 0.8 was used because it was the smallest value to produce a clean white matter mask, while maintaining most of the important white matter structures, such as the internal and external capsules, that are variable between individuals [14]. To create the dataset level white matter mask only subjects within that dataset are used, and to create the cross dataset white matter mask all subjects are used. All images were masked and spatially smoothed using a 4mm half maximum Gaussian kernel to increase the signal to noise ratio and improve across subject analyses.

Voxel-Wise Correlations

Each 4D image was reshaped in 2D (spatial coordinates x timeseries). The first 10 seconds of each image were removed to ensure scanner magnetization reached steady state. A voxel level Pearson correlation coefficient was calculated for each scan using the mean time series signal at each volume for each scan. All scan correlations were then averaged across all subjects within a dataset.

Clustering

The white matter voxel correlations underwent hierarchical clustering using MATLAB's pdist, linkage, and clusterdata functions [19] [20]. The difference in the voxel correlations were measured using the metric one minus the Pearson correlation coefficient where the Pearson correlation coefficient is the correlation between two voxel correlations. These differences were then clustered by minimizing the unweighted averages of the difference. Clustering was performed on hierarchical levels of 2 through 50 to create parcellations. The number of clusters in a parcellation is equal to the hierarchical level.

Clustering was investigated within each dataset and between datasets. To evaluate the stability of clustering within a dataset, the dataset specific white matter mask was applied. Five-fold cross validation was used where each subject and all the scans associated with that subject were randomly assigned into one of 5 folds. Clustering was performed independently within each fold. The clusters were compared to each other using the mean of Dice Coefficients between paired clusters. Since cluster labels are assigned arbitrarily to each cluster, to compare clusters the corresponding clusters must be matched. All clusters in one parcellation were compared to all clusters in another parcellation. The pair of clusters with the largest Dice Coefficient is considered a match and removed from future possible pairings. This process was repeated until all clusters were matched. The stability of two parcellations is measured as the mean Dice Coefficient.

Permutation testing was performed on each dataset to evaluate if the clusters are exchangeable (H_0: defined clusters are exchangeable). Using 5-fold cross validation, clusters in each fold were randomly permuted 1000 times and the observed mean Dice Coefficients from the random parcellations were compared to the observed mean Dice Coefficients from the original 5-fold validation in each dataset.

Likewise, to evaluate the reproducibility of the clustering across datasets, the cross dataset white matter mask was applied. Clustering was completed independently in a dataset using all the subjects from that dataset. The stability between the parcellations was compared using the mean Dice Coefficient. To identify clusters which are similar across datasets, the number of times a cluster appears within both datasets, as well as the mean Dice Coefficient between the clusters is recorded. The clusters that appear most frequently in multiple datasets are investigated. These frequent and similar clusters are then compared with regions defined by the JHU-DTI-SS Type 1 Atlas [21] and the Brodmann Atlas [22] [23] using the same Dice Coefficient pairing scheme.

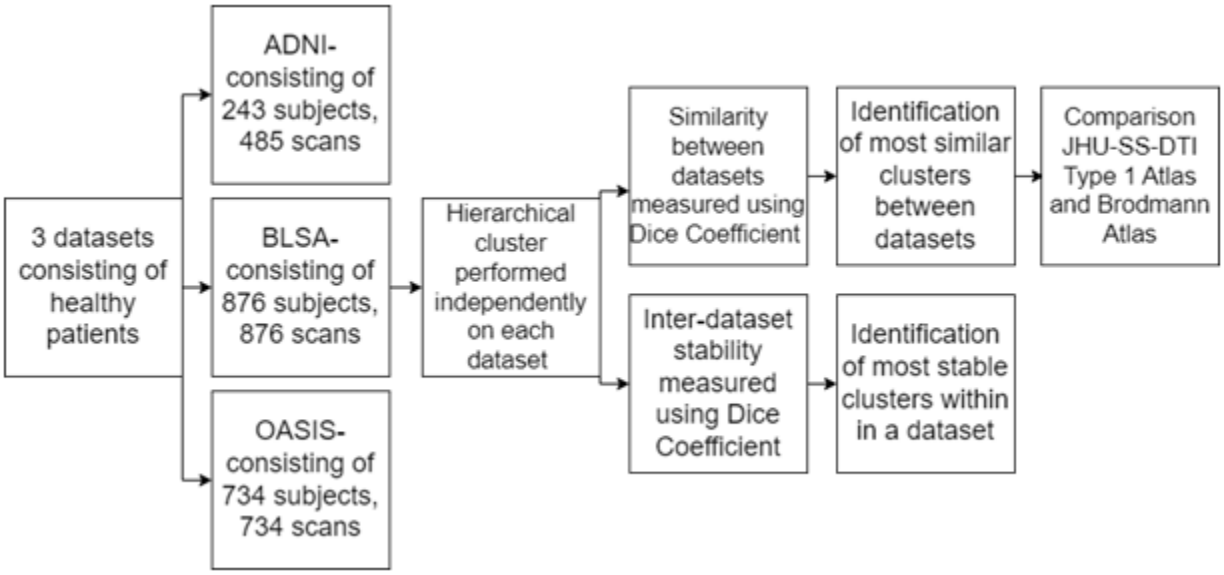

Figure 2 Experimental Design. The experimental design to assess the reproducibility of hierarchical clustering resting state white matter. Three different datasets, ADNI, BLSA, and OASIS, from different data collection sites were used. Hierarchical clustering with hierarchical levels from 2 to 50 was performed independently within each dataset. To compare within dataset clustering, 5-fold cross validation by subject populations was used with the stability being the mean Dice Coefficient. To compare the similarity of the clustering between two different datasets the number of times clusters appear in more than one dataset is recorded and the similarity between datasets is measured as the mean Dice Coefficient. Additionally, the most similar clusters are compared to the JHU-SS-DTI Type 1 Atlas and Brodmann Atlas.

RESULTS

Clustering Stability Within Dataset

Investigating the stability of the clustering within each dataset from the 5-fold cross validation resulted in hierarchical levels that have local maximum mean Dice Coefficients. At these local maximums, the clustered regions are more similarly clustered, or more stable, across the validation sets. The more stable levels differ across the datasets; however, in each dataset there is a more stable parcellation at a lower, middle, and larger hierarchical level (Figure 3). The ANDI and OASIS datasets cluster symmetrically, with the mean Dice Coefficients between regions in the left and right hemispheres all greater than 0.85. The BLSA dataset is not symmetric in clustering. Permutation testing of the clusters in each dataset suggests that the clusters are not exchangeable at any hierarchical level ($P < 0.001$), suggesting the clustering parcellation is unique to the data.

Investigating the smaller parcellations, in the ADNI dataset the major lobe regions- frontal, occipital, temporal, and parietal- are defined. In the OASIS dataset, the lobe regions are not as clearly defined, but the clusters are still exhibiting a cluster in each lobe. As the number of parcellations increases, more clusters appear within the frontal and temporal lobes in both the OASIS and ADNI datasets. The frontal and temporal lobes are responsible for memory, sensory, and language processing, which are all expected to be activated during resting state scans. The frontal lobe is also responsible for fine motor movement, which includes tongue and eye movements most likely still occurring in resting state scans. In the larger parcellations for the OASIS and ANDI datasets, the brainstem is identified and clusters within the midbrain are more defined. In BLSA, the brainstem is defined in the lower parcellations. As the parcellations increase, the frontal lobe and midbrain have more clusters, while the

temporal lobe has fewer clusters. However, the midbrain region should also be activated during resting state, so clusters within the midbrain are not unexpected (Figure 4).

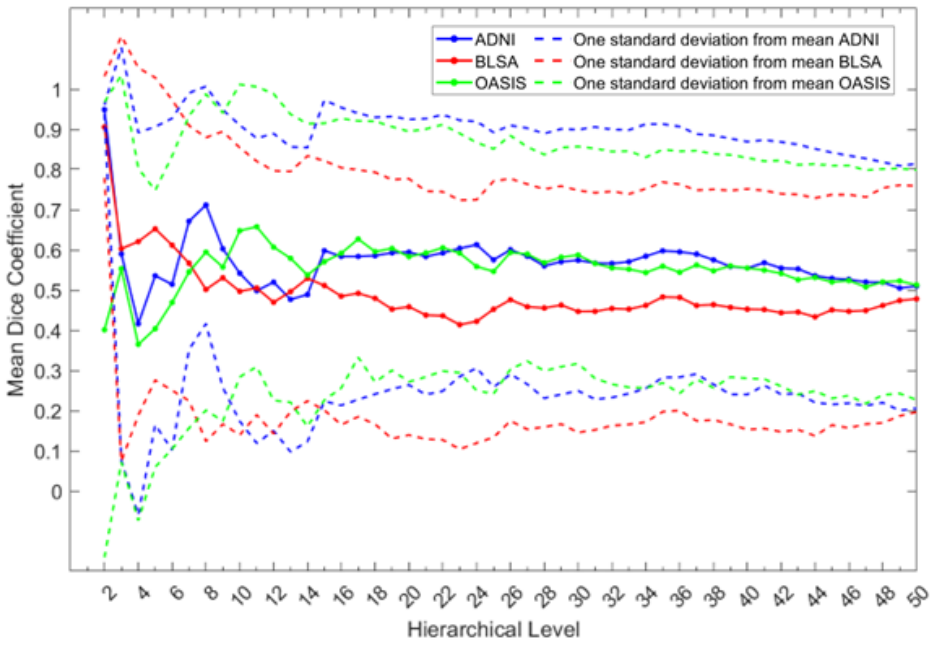

Figure 3 Within Dataset Cluster Stability. As hierarchical level increases, the parcellations become relatively stable in each dataset. For each dataset, there are hierarchical levels which have local larger mean Dice Coefficients, indicating more stable clusters. Each of the datasets has more stable clusters at similar hierarchical levels (ADNI n = 5, 8, 12, 15, 18, 24, 26, 35; BLSA n = 5, 9, 14, 17, 26, 36; OASIS n = 3, 8, 11, 14, 17, 26, 30), suggesting that the parcellations are capturing similar white matter signals.

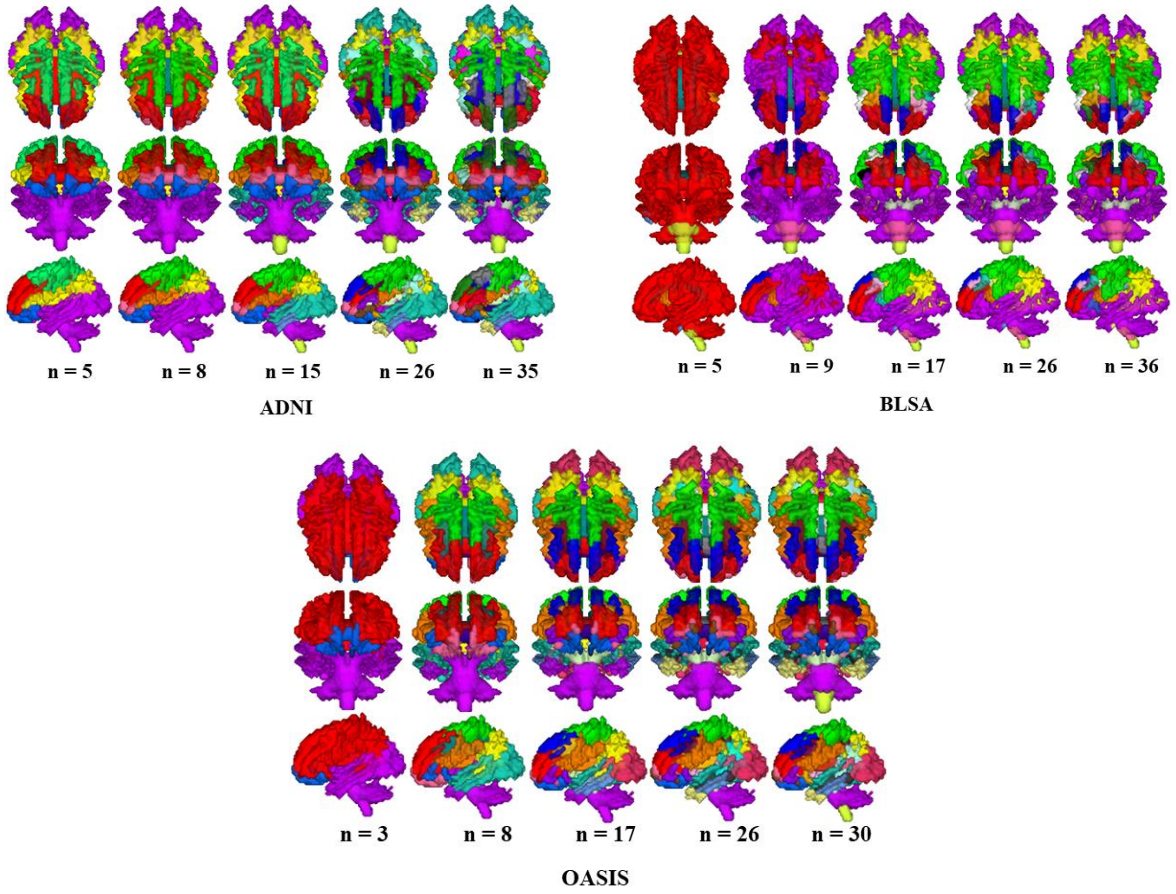

Figure 4. Visualization of Stable Clusters. Visualization of the more stable parcellations at different parcellation levels shows there are clear differences between each of the datasets. ADNI and OASIS are symmetric and as the parcellation number increases, more regions in the frontal and temporal lobe are defined. BLSA is not symmetric and identifies the brainstem at smaller parcellations. In larger parcellations regions of OASIS and ADNI, the frontal and temporal lobe become more clustered, while in BLSA the frontal lobe and midbrain become more clustered.

Cluster Reproducibility Across Datasets

Investigating the reproducibility of the clustering across the datasets results in relatively low mean Dice Coefficients. However, there are parcellations with local maximum mean Dice Coefficients, indicating more similarities between the two datasets being compared at that hierarchical level (Figure 5). When comparing the clusters within a dataset that have more similar cluster parcellations between datasets, there are specific similar clusters that consistently appear across different hierarchical levels. ADNI and OASIS parcellations have regions of the brain with much larger similarities (Dice Coefficient greater than 0.80) compared to the cluster similarities between ADNI and BLSA or OASIS and BLSA.

Looking specifically at the similarities between OASIS and BLSA, there is a cluster in the parietal lobe region and deep in the temporal lobe region. These clusters are also found when comparing ANDI and BLSA clusters. Likewise, investigations into the similarities between OASIS and ADNI finds that the midbrain region is similarly defined. The midbrain is also defined when comparing clusters between ADNI and BLSA. All comparisons have the brainstem identified well (larger mean Dice Coefficient), and all comparisons identify a cluster in the posterior region of the brain across the left and right hemispheres. Additional similar regions identified between clusters are all located in the frontal and temporal lobes, which are the lobes most likely to be activated during resting state scans. The similarities

between the datasets indicate that specific white matter parcellations may have specific clusters that provide meaningful information that is reproducible across datasets (Figure 6).

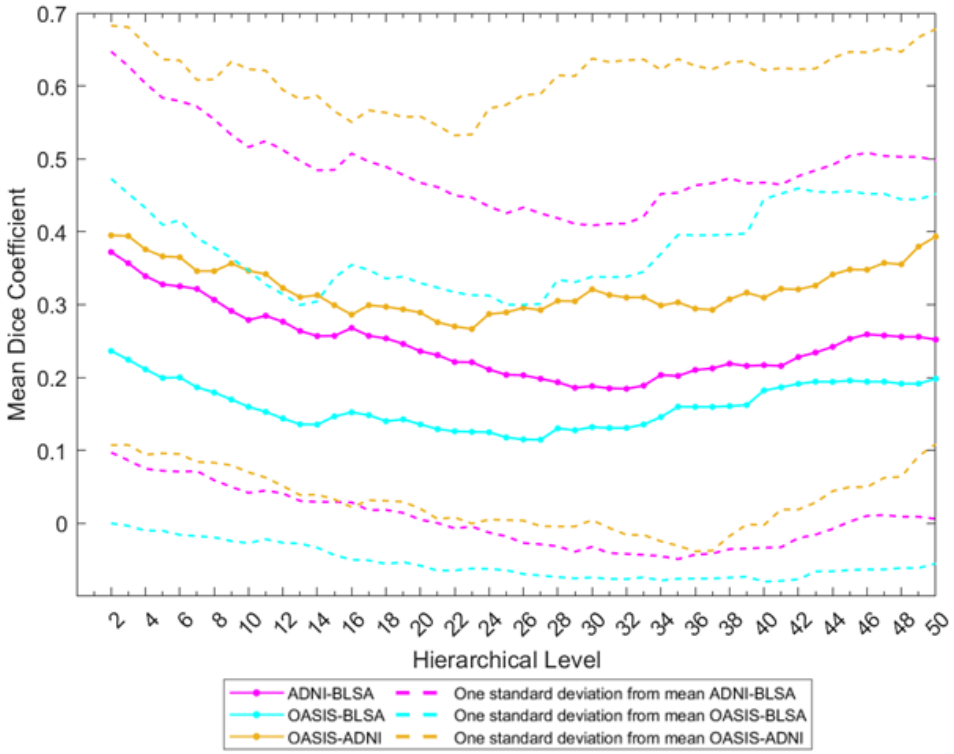

Figure 5. Cluster Similarity Between Datasets. The mean Dice Coefficient measuring the similarity of the clustering between datasets is low, suggesting hierarchical clustering differs between each dataset. There are regions of local maximum mean Dice Coefficients, indicating there are parcellations that have regions that are more similar between datasets.

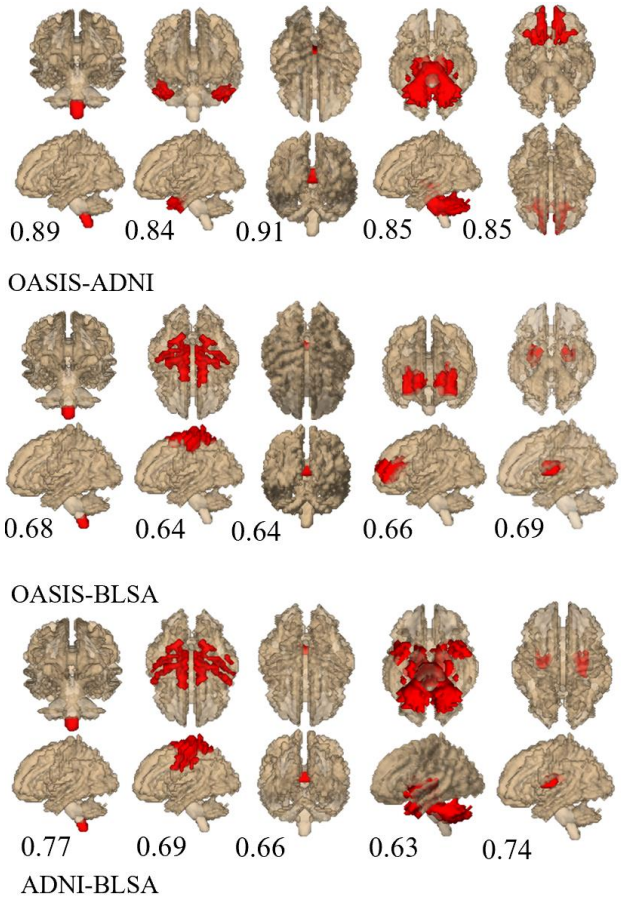

Figure 6. Visualization of Similar Clusters. There are clustered regions that when comparing datasets, have larger Dice Coefficients and appear consistently across hierarchical levels. Many of the regions appear in the temporal lobe, which is expected to be activated during resting state. The brainstem is identified in all datasets. A cluster in the posterior region of the brain across the two hemispheres of the brain is also identified across all datasets. These similarities across the datasets suggest that specific clusters of white matter voxels provide meaningful information that is reproducible across datasets.

Comparison to Atlases

The identified similar clusters, or networks, have low Dice Coefficients when comparws to the Brodmann Atlas. This suggests that the white matter functional parcellations are different than the cellular based regions defined by the Brodmann Atlas. The functional networks compared to the structural regions in the JHU-DTI-SS Type 1 Atlas, find that the internal capsules and middle fronto-orbital gyrus are captured well by a cluster. Also, the corpus callosum and medulla are captured across all three datasets. These regions are responsible for sensory processing and transmitting information across brain regions and will remain active during resting state scans. Although all resting state white matter clusters are not reproducible, regions of the brain which may be active during resting state scans cluster similarly between subject populations and different acquisition sites, suggesting there are meaningful specific white matter signal correlations in BOLD-fMRI resting state scans (Figure 7).

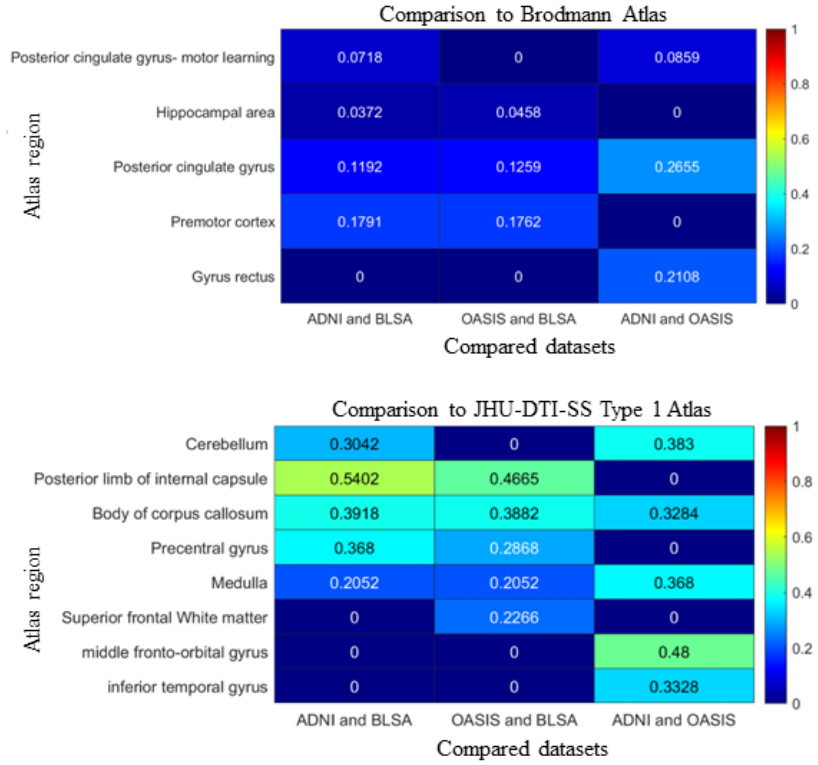

Figure 7. Comparison to Cellular and Structural Atlases. Comparing the identified networks to the Brodmann Atlas (top) the Dice Coefficients are low. Comparing to the JHU-DTI-SS Type 1 Atlas (bottom) all regions between datasets capture a portion of the corpus callosum and medulla which should be activated during resting state. The internal capsules and middle fronto-orbital gyrus are captured well by the intersection of certain dataset regions. Brain regions that may be activated during rest cluster similarly across datasets.

DISCUSSION

In this work, hierarchical clustering of white matter BOLD signals produces similar cluster patterns across different subject populations and different image acquisition sites. Although white matter clusters are not truly reproducible, the most stable parcellations within each dataset occur at similar hierarchical levels, suggesting there are specific organizations of the white matter signals that better define the white matter correlations compared to other white matter signal organizations. Additionally, clustering revealed specific clusters that are similarly defined across subject populations and acquisition sites which are consistent with expected resting state white matter activation.

Comparing to the Brodmann Atlas and JHU-DTI-SS Type 1 Atlas indicates that the functional parcellations differ from the structural and cellular based regions. However, the most similar regions within the JHU-DTI-SS Type 1 Atlas are regions of the brain that would be activated during resting state scans. This suggests that the white matter signal clusters, which are similar across datasets, may provide unique information that is similar in all datasets, creating a ‘default white matter network’, in a similar manner to the default grey matter network. This work is limited to resting state white matter scans only. Future work should investigate the clustering of white matter using different clustering methods and compare to task based white matter signals.

REFERENCES

[1] Nair, D. G., "About being bold," Brain Research Reviews **50**(2), 229–243 (2005).

[2] Logothetis, N. K., "Neurovascular uncoupling: Much ado about nothing," Frontiers in Neuroenergetics **2** (2010).

[3] Fox, M. D., Snyder, A. Z., Vincent, J. L., Corbetta, M., Van Essen, D. C.., Raichle, M. E., "The human brain is intrinsically organized into dynamic, anticorrelated functional networks," Proceedings of the National Academy of Sciences **102**(27), 9673–9678 (2005).

[4] Tsvetanov, K. A., Henson, R. N., Jones, P. S., Mutsaerts, H., Fuhrmann, D., Tyler, L. K.., Rowe, J. B., "The effects of age on resting-state bold signal variability is explained by cardiovascular and cerebrovascular factors," Psychophysiology **58**(7) (2020).

[5] Kazemifar, S., Manning, K. Y., Rajakumar, N., Gómez, F. A., Soddu, A., Borrie, M. J., Menon, R. S.., Bartha, R., "Spontaneous low frequency bold signal variations from resting-state fmri are decreased in alzheimer disease," PLOS ONE **12**(6) (2017).

[6] Schilling, K. G., Li, M., Rheault, F., Ding, Z., Anderson, A. W., Kang, H., Landman, B. A.., Gore, J. C., "Anomalous and heterogeneous characteristics of the bold hemodynamic response function in white matter," Cerebral Cortex Communications **3**(3) (2022).

[7] Gore, J. C., Li, M., Gao, Y., Wu, T.-L., Schilling K. G., Huang, Y., Mishra, A., Newton, A. T., Rogers, B. P., et al., "Functional MRI and resting state connectivity in white matter - a mini-review," Magnetic Resonance Imaging **63**, 1–11 (2019).

[8] Fraser, L. M., Stevens, M. T., Beyea, S. D.., D'Arcy, R. C., "White versus gray matter: Fmri hemodynamic responses show similar characteristics, but differ in peak amplitude," BMC Neuroscience **13**(1) (2012).

[9] Peer, M., Nitzan, M., Bick, A. S., Levin, N.., Arzy, S., "Evidence for functional networks within the human brain's white matter," The Journal of Neuroscience **37**(27), 6394–6407 (2017).Jiang, C., Cai, S.., Zhang, L., "Functional connectivity of white matter and its association with sleep quality," Nature and Science of Sleep **Volume 15**, 287–300 (2023).

[10] LaMontagne, P. J., Benzinger, T. LS., Morris, J. C., Keefe, S., Hornbeck, R., Xiong, C., Grant, E., Hassenstab, J., Moulder, K., et al., Oasis-3: Longitudinal neuroimaging, clinical, and cognitive dataset for normal aging and alzheimer disease (2019).

[11] The Alzheimer's Disease Neuroimaging Initiative (ADNI)* Jack Jr CR, Bernstein MA, Fox NC, et al. The Alzheimer's disease neuroimaging initiative (ADNI): MRI methods. Journal of Magnetic Resonance Imaging: An Official Journal of the International Society for Magnetic Resonance in Medicine. 2008;27(4):685-691

[12] Ferrucci, L. (2008). The Baltimore Longitudinal Study of Aging (BLSA): A 50-year-long journey and plans for the future [Editorial]. *The Journals of Gerontology: Series A: Biological Sciences and Medical Sciences, 63*(12), 1416–1419. https://doi.org/10.1093/gerona/63.12.1416

[13] Gao, Y., Lawless, D. R., Li, M., Zhao, Y., Schilling, K. G., Xu, L., Shafer, A. T., Beason-Held, L. L., Resnick, S. M., et al., "Automatic preprocessing pipeline for white matter functional analyses of large-scale databases," Medical Imaging 2023: Image Processing (2023).

[14] Yan, C.-G., Wang, X.-D., Zuo, X.-N.., Zang, Y.-F., "DPABI: Data Processing & analysis for (resting-state) brain imaging," Neuroinformatics **14**(3), 339–351 (2016).

[15] Friston, K. J., "Functional and effective connectivity in neuroimaging: A synthesis," Human Brain Mapping **2**(1–2), 56–78 (1994).

[16] Gaser, C., Dahnke, R., Thompson, P. M., Kurth, F.., Luders, E., Cat – a computational anatomy toolbox for the analysis of structural MRI Data (2022).

[17] Power, J. D., Mitra, A., Laumann, T. O., Snyder, A. Z., Schlaggar, B. L.., Petersen, S. E., "Methods to detect, characterize, and remove motion artifact in resting state fmri," NeuroImage **84**, 320–341 (2014).

[18] The MathWorks, Inc., linkage (2011).

[19] The MathWorks, Inc., clusterData (2011).

[20] Oishi, K., Faria, A., Jiang, H., Li, X., Akhter, K., Zhang, J., Hsu, J. T., Miller, M. I., van Zijl, P. C. M., et al., "Atlas-based whole brain white matter analysis using large deformation diffeomorphic metric mapping: Application to normal elderly and alzheimer's disease participants," NeuroImage **46**(2), 486–499 (2009).

[21] NeuroImaging Tools and Resources Collaboratory, Mricon.

[22] Zilles, Karl. "Brodmann: a pioneer of human brain mapping-his impact on concepts of cortical organization." *Brain : a journal of neurology* vol. 141,11. 3262-3278. doi:10.1093/brain/awy273 (2018)